RAPID COMMUNICATIONS

PHYSICAL REVIEW A VOLUME 39, NUMBER 7 APRIL 1, 1989

Nonlinear standing waves in Couette-Taylor flow

Randall Tagg, W. Stuart Edwards, and Harry L. Swinney
Center for Nonlinear Dynamics and the Department of Physics, University of Texas, Austin, Texas 78712

Philip S. Marcus
Department of Mechanical Engineering, University of California, Berkeley, California 94720
(Received 4 November 1988)

A nonlinear stability analysis by Demay and Iooss [J. Mec. Theor. Appl., special issue, p. 193 (1984)] of flow between concentric rotating cylinders (the Couette-Taylor system) predicted a transition from the basic flow to a state with ribbons, which are traveling waves in the azimuthal direction but standing waves in the axial direction. We have observed the transition to ribbons in laboratory experiments and numerical simulations, and the measured wave speeds are in accord with those obtained numerically.

The Couette-Taylor system has served as a paradigm for testing ideas on stability in systems described by nonlinear partial differential equations since the landmark work of Taylor[1] on flow between concentric rotating cylinders. He measured the critical Reynolds number for the primary instability and showed that it agreed within a few percent with the predictions of a linear stability analysis. This was the first quantitative agreement of theory and experiment for *any* flow instability. However, *linear* stability analyses do not, in general, completely determine the final pattern of secondary flow. Our experiments and numerical simulations demonstrate the existence of a secondary flow that was first found to be possible from a nonlinear analysis[2] two decades ago but was only recently predicted to be stable.[3]

The symmetry of the Couette-Taylor system induces degeneracies in the linear eigenmodes and only a *nonlinear* calculation can determine the combination of modes that produces stable patterns. Two possible flows for strongly counter-rotating cylinders are *spirals* with opposite helicities; these modes, which are traveling waves in the axial and azimuthal directions, were observed by Taylor and, subsequently, by others.[4-6] In a nonlinear analysis DiPrima and Grannick[2] later found a third mode, but it was unstable for the parameters they considered. This mode, which is to lowest order a superposition of the two spirals, is a standing wave in the axial direction and traveling wave in the azimuthal direction. Recently, Demay and Iooss[3] have examined this mode, which they call *ribbons*. They used a center-manifold formalism[7] to reduce the Navier-Stokes equations to a set of coupled ordinary differential equations, and coefficients in these Landau equations were computed as a function of the control parameters. Calculations for a radius ratio of 0.752 yielded stable ribbons over a finite range of cylinder speeds, while at the other radius ratio considered, 0.950, the ribbon state was not stable.

Our experiments confirm the existence of ribbons at a set of parameter values where Demay and Iooss found the transition to be subcritical; at these values their perturbation analysis could not determine the final form of the secondary flow. Therefore, to corroborate our observations we undertook direct numerical simulations of the Navier-Stokes equations at the parameter values for which ribbons were observed; the simulations confirm the existence of a subcritical transition to ribbons.

We now describe the analysis that leads to the coupled complex Landau equations studied by Iooss and coworkers,[3,7] and then we will describe our observations and simulations.

Consider a system with inner cylinder radius a, outer radius b, and corresponding angular velocities Ω_1 and Ω_2. The dimensionless control parameters are the Reynolds numbers $R_1=(b-a)a\Omega_1/\nu$, where ν is the kinematic viscosity. Couette flow (the basic flow), which is stable for sufficiently small R_1, is given by $\mathbf{U}_0=(Ar+B/r)\mathbf{e}_\theta$, where A and B are determined by the no-slip boundary conditions at the cylinder walls. For fixed a/b and R_2, instability is observed upon slow ramping of R_1 through a critical value R_{1c}. The eigenmodes for the nonaxisymmetric linear stability problem are perturbations to Couette flow of the form

$$\mathbf{u}_L(r,\theta,z)e^{(\sigma+i\omega)t}=\mathbf{F}(r)e^{i(kz+m\theta+\theta_L)}e^{(\sigma+i\omega)t}, \quad (1)$$

$$\mathbf{u}_R(r,\theta,z)e^{(\sigma+i\omega)t}=S\mathbf{F}(r)e^{i(-kz+m\theta+\phi_R)}e^{(\sigma+i\omega)t}, \quad (2)$$

where L and R refer to left- and right-handed spirals, and the vector field $S\mathbf{F}(r)$ is obtained from $\mathbf{F}(r)$ by reflection through the plane $z=0$. The phases ϕ_L and ϕ_R are arbitrary. At R_{1c} the growth rate σ is zero and the axial wave number k and azimuthal wave number m take the values k_c and m_c. These values[8] are used as input to both the nonlinear analysis and the numerical simulations.

Following Demay and Iooss, the perturbation of the flow can be written as

$$\mathbf{u}=A\mathbf{u}_L+\bar{A}\bar{\mathbf{u}}_L+B\mathbf{u}_R+\bar{B}\bar{\mathbf{u}}_R+\mathbf{u}'(r,\theta,z;\epsilon,A,\bar{A},B,\bar{B}), \quad (3)$$

where the overbar denotes complex conjugate and $\epsilon=(R_1-R_{1c})/R_{1c}$. The residual field $\mathbf{u}'$ is spatially periodic with axial and azimuthal wave numbers k_c and m_c, respectively, and can be expressed as a power-series expansion in ϵ, A, $\bar{A}$, B, and $\bar{B}$. The complex amplitudes

A and B are governed by the coupled Landau equations:

$$dA/dt=(\sigma+i\omega)A-(g|A|^2+h|B|^2)A+\cdots, \quad (4)$$

$$dB/dt=(\sigma+i\omega)B-(g|B|^2+h|A|^2)B+\cdots, \quad (5)$$

where $\sigma=\sigma_1\epsilon$ and $\omega=\omega_c+\omega_1\epsilon$. The coefficients σ_1, ω_1, $g=g_r+ig_i$, and $h=h_r+ih_i$ depend on the control parameters R_2 and a/b in a way that may be computed numerically.[3] Large-scale modulation of the amplitudes has been neglected; the system is assumed to be exactly periodic in z. The three solutions to Eqs. (4) and (5) correspond to

$$|A|=(\sigma_1\epsilon/g_r)^{1/2}, \quad B=0 \text{ (left spiral)}, \quad (6)$$

$$A=0, \quad |B|=(\sigma_1\epsilon/g_r)^{1/2} \text{ (right spiral)}, \quad (7)$$

and

$$|A|=|B|=[\sigma_1\epsilon/(g_r+h_r)]^{1/2} \text{ (ribbons)}. \quad (8)$$

Spirals are supercritical and stable when $g_r>0$ and $h_r/g_r>1$; ribbons are supercritical and stable for $g_r>0$ and $-1<h_r/g_r<1$. Spirals are subcritical for $g_r<0$ and ribbons for $h_r<-g_r$.

Figure 1 shows the linear stability result (for $a/b=0.727$) for the primary transition boundary in the R_2-R_1 plane with $R_2<0$. The boundary is divided into sections of differing azimuthal wave number m. The section for $m=2$ is further subdivided according to the nonlinear theory into regions of supercritical spirals, supercritical ribbons, and subcritical transition. The key finding is that ribbons *exist*. However, we have observed robust ribbons only where the theory predicts the transition to be subcritical.

Our laboratory[9] and numerical results concentrate around the parameter values $a/b=0.727$, $R_2=-340$,

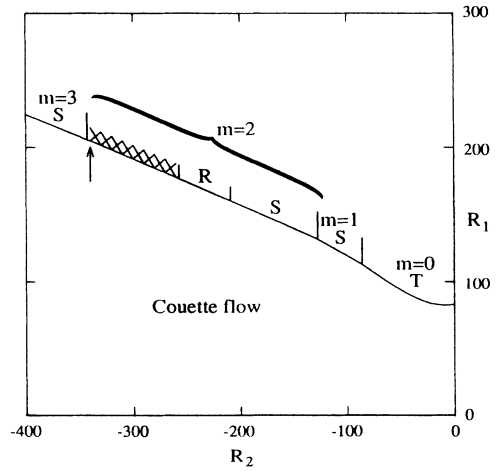

FIG. 1. Primary transition boundary for $a/b=0.727$, showing segments predicted by linear stability theory (Ref. 8) to have different values of m. The secondary flows predicted by nonlinear theory are as follows: T—Taylor vortices, S—spirals, R—ribbons. The cross-hatch marks indicate where the transition is predicted to be subcritical. The parameters investigated by experiment and numerical simulation are shown by a vertical arrow.

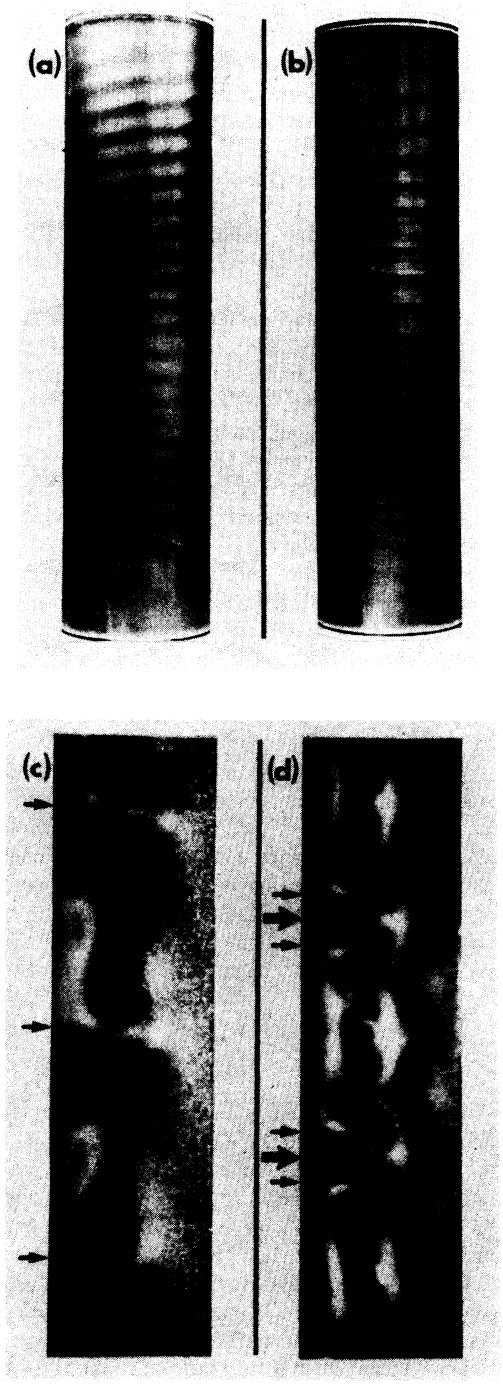

FIG. 2. Spiral flow at $R_1=152$ and $R_2=-175$ is shown in (a) frontal and (c) cross-sectional views one-half period apart in time. Ribbon flow at $R_1=207$ and $R_2=-340$ is shown in (b) frontal and (d) cross-sectional views one-half period apart in time; strong vortices are paired near an outflow jet, as indicated by the large arrows in (d). Small arrows indicate vortex centers. The cross-sectional views were obtained by illuminating the gap between the cylinders with a light sheet; to improve contrast and decrease the lensing effect the light sheet was placed at an angle of about 45° to the r-z plane.

and $R_{1c}=204.9$. Photographs of spirals are shown in Figs. 2(a) and 2(c) and ribbons in Figs. 2(b) and 2(d). In Fig. 2(a) spirals of opposite helicity can be seen to meet in the center of the cylinder. In Fig. 2(b) the ribbons exhibit a horizontal banded structure with an interleaved or "checkerboard" pattern traveling around the cylinders. It is apparent in photographs of radial cross sections that the ribbons are reflection symmetric while the spirals are not [cf. Fig. 2(c) with 2(d)]. Note that the spirals have one strong vortex per axial wavelength, an asymmetry that is strictly a nonlinear effect.

Three-dimensional numerical simulations of the full incompressible Navier-Stokes equations were performed with a pseudospectral code.[10] The code imposes an azimuthal periodicity $\mathbf{u}(r,\theta,z)=\mathbf{u}(r,\theta+2\pi/m_c,z)$ and an axial periodicity $\mathbf{u}(r,\theta,z)=\mathbf{u}(r,\theta,z+2\pi/k_c)$.[11] The stability of solutions was tested by perturbing the converged solution with $\mathbf{u}_L$, by starting with random noise, and by starting with a state formed of equal amplitude spiral linear eigenmodes $\mathbf{u}_L$ and $\mathbf{u}_R$.

Figure 3 shows plots of the numerically determined velocity field for ribbons. The $\theta-z$ projection in Fig. 3(a) clearly exhibits the checkerboard symmetry apparent in the photograph in Fig. 2(c): $\mathbf{u}(r,\theta,z)=\mathbf{u}(r,\theta\pm\pi/m_c,z\pm\pi/k_c)$. Moreover, the $r-z$ projections in Fig. 3(b) match the laboratory observation that the vortex centers are near the radial outflow jet; a pure superposition of the linear eigenmodes does not show this effect. The pair of $r-z$ projections shows one vortex pair being replaced by an identical vortex pair a half an axial wavelength away; the outflow jet reverses into a weak inflow. In contrast, in spiral flow the single dominant vortex travels continuously up the axis, followed by the next such vortex one full axial wavelength behind. The strong radial outflow of the ribbons is correlated with an increase in the azimuthal velocity, as evidenced by the outward bulge in the contours of $u_\theta=0$. This mechanism transports angular momentum outward from the inner cylinder, increasing torque above that of Couette flow.

The numerical simulation confirms that the transition to ribbons is weakly subcritical at the parameter values studied. The computed wave speeds agree with those measured to within 1%, and both are 1.6% or greater than the linear stability wave speed at onset. Ribbons were computed down to $\epsilon=1.46\times10^{-3}$ and the turning point, $\epsilon=-2.44\times10^{-3}$, was estimated from an analysis of the computed amplitude as a function of R_1. No hysteresis was observed in experiments with a resolution $\Delta\epsilon\approx1\times10^{-3}$, but the experimental transition could be continuous as a consequence of finite-size effects.

Thus the laboratory experiments and numerical simulations confirm the existence of ribbons. However, an attempt to observe a *supercritical* transition to ribbons in experiments at $R_2=-230$, where the transition is predicted to be supercritical, was not successful—only spirals were found. Although simulations yielded a transition to ribbons at $R_2=-230$, slightly above the onset of ribbons,

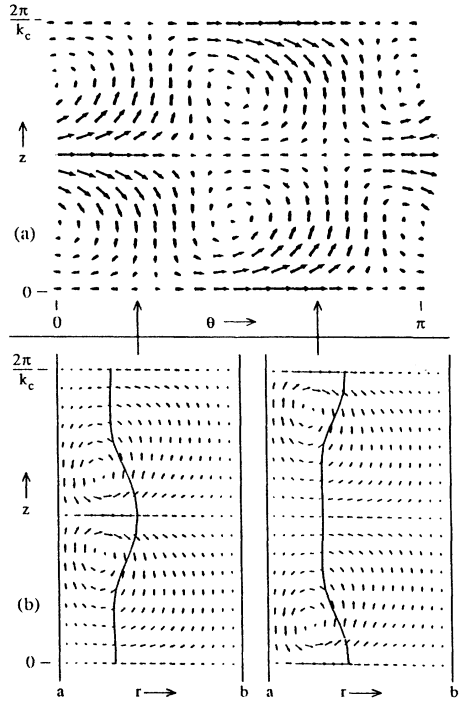

FIG. 3. The numerically computed velocity field for $R_2=-340$ and $\epsilon=1.02\times10^{-2}$: (a) θ-z projection for $r=(a+b)/2$. (b) r-z projections for θ values indicated by arrows in (a). The curve in each projection is the contour $u_\theta=0$.

at $\epsilon=1.46\times10^{-2}$, a *spiral* rather than a ribbon state was obtained; this spiral was robust under perturbations. This nearby stable spiral state may explain the difficulty in experimentally observing ribbons at this value of R_2. Another explanation may be that end effects in the laboratory system result in a transition that is different from that given by the theory and numerical simulations, both of which assume axial periodicity. Even in the observed ribbons state at $R_2=-340$ there is a definite departure from axial periodicity: The amplitude of the pattern decreases towards the ends of the cylinder, and faint spirals rather than ribbons are observed there. Furthermore, recent theory[12] and experiments[13] on convection indicate that end effects can lead to dynamics that depend fundamentally on the finite size of a system. An investigation of ribbons in which finite cylinder size is taken into account is now underway.

The authors thank B. Dornblaser, G. Flynn, D. Hirst, H. King, E. Kostelich, and Q. McCarty for their help. This research was supported by the Office of Naval Research Nonlinear Dynamics program. Computational resources were provided by the University of Texas Center for High Performance Computing.

[1]G. I. Taylor, Philos. Trans. R. Soc. London Ser. A **223**, 289 (1923).

[2]R. C. DiPrima and R. N. Grannick, in *Instability of Continuous Systems,* edited by H. Leipholz (Springer, Berlin, 1971), p. 55.

[3]Y. Demay and G. Iooss, J. Mec. Theor. Appl., special issue, p. 193 (1984). The predictions have been corrected to our radius ratio using results from Demay's code.

[4]D. Coles, J. Fluid Mech. **21**, 385 (1965).

[5]H. A. Snyder, Phys. Fluids **11**, 728 (1968); **11**, 1599 (1968); Int. J. Non-Linear Mech. **5**, 659 (1970). Snyder's detailed study of the primary transition to nonaxisymmetric modes found both spirals and "puffing cells." It is not clear from the published data whether or not the latter can be identified with ribbons.

[6]C. D. Andereck, S. S. Liu, and H. L. Swinney, J. Fluid Mech. **164**, 155 (1986).

[7]P. Chossat and G. Iooss, Jpn. J. Appl. Math. **2**, 37 (1985).

[8]A tabulation of R_{1c}, k_c, m_c, and ω_c as a function of a/b and R_2 has been given in W. F. Langford, R. Tagg, E. J. Kostelich, H. L. Swinney, and M. Golubitsky, Phys. Fluids **31**, 776 (1988).

[9]In our apparatus, $a=5.657$ cm, $b=7.779$, Γ (aspect ratio) $=36$, and the working fluid was a mixture (by weight) of 65% glycerol, 34% water, and 1% Kalliroscope AQ1000 "rheoscopic concentrate" used for flow visualization. Wave speeds were determined from the period of oscillation of the intensity of scattered laser light.

[10]P. S. Marcus, J. Fluid Mech. **146**, 45 (1984); **146**, 65 (1984).

[11]We used 32 Fourier modes in z and θ and 33 Chebyshev modes in the radial direction. Each time step was 0.0018 times the inner-cylinder period. The numerical solution was considered to have converged when the computed torque at all 33 radial collocation points was the same to within 5 parts per million. Convergence times were of the order of tens of inner cylinder periods.

[12]M. C. Cross, Phys. Rev. Lett. **57**, 2935 (1986); A. E. Deane, E. Knobloch, and J. Toomre, Phys. Rev. A **37**, 1817 (1988); M. Bestehorn, R. Friedrich, and H. Haken, Z. Phys. B **72**, 265 (1988).

[13]J. Fineberg, E. Moses, and V. Steinberg, Phys. Rev. Lett. **61**, 838 (1988); P. Kolodner and C. M. Surko, *ibid.* **61**, 842 (1988).

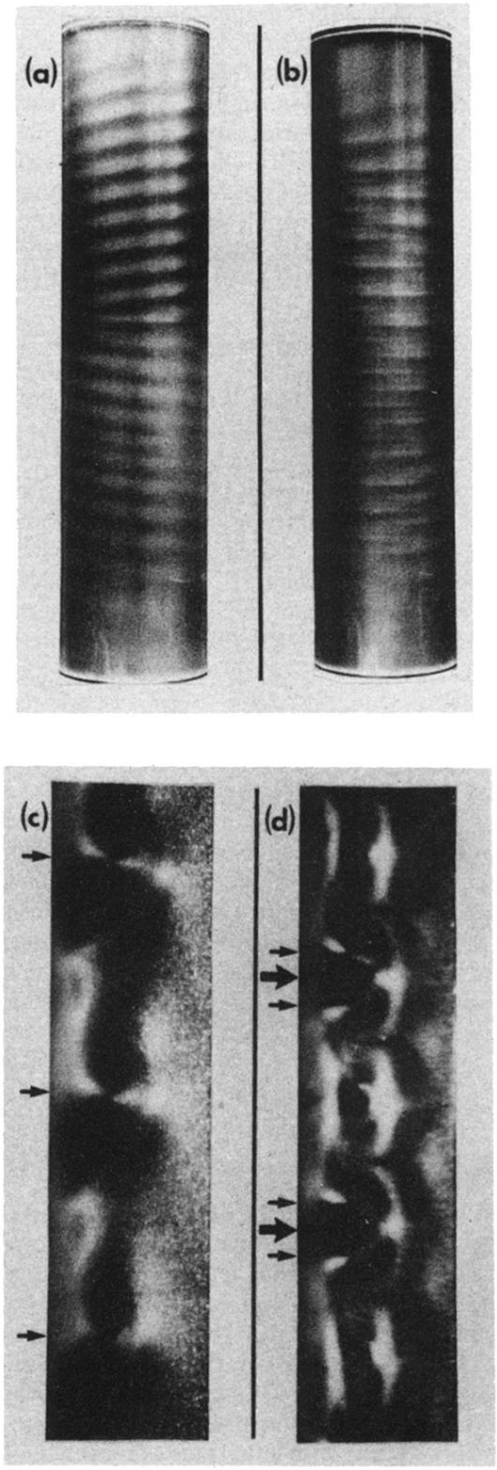

FIG. 2. Spiral flow at $R_1 = 152$ and $R_2 = -175$ is shown in (a) frontal and (c) cross-sectional views one-half period apart in time. Ribbon flow at $R_1 = 207$ and $R_2 = -340$ is shown in (b) frontal and (d) cross-sectional views one-half period apart in time; strong vortices are paired near an outflow jet, as indicated by the large arrows in (d). Small arrows indicate vortex centers. The cross-sectional views were obtained by illuminating the gap between the cylinders with a light sheet; to improve contrast and decrease the lensing effect the light sheet was placed at an angle of about 45° to the r-z plane.